Transport and Communications Science Journal, Vol. 76, Issue 04 (05/2025), 583-596

Transport and Communications Science Journal

MECHANICAL CHARACTERIZATION OF AMORPHOUS SILICA MATERIAL AND NANOPARTICLE FORMATION VIA COMPUTATIONAL APPROACH

Le Tien Thinh[1,2*], Duong Thanh Huan[3]

[1] Phenikaa University, Nguyen Trac Street, Hanoi, Vietnam

[2] Phenikaa Research and Technology Institute, No 167 Hoang Ngan Street, Hanoi, Vietnam

[3] Vietnam National University of Agriculture, No 86 Trau Quy Street, Hanoi, Vietnam

ARTICLE INFO

TYPE: Research Article
Received: 13/03/2025
Revised: 15/04/2025
Accepted: 09/05/2025
Published online: 15/05/2025
https://doi.org/10.47869/tcsj.76.4.11
[*] *Corresponding author*
Email: thinh.letien@phenikaa-uni.edu.vn; Tel: +84902889339

Abstract. Amorphous silica is widely used in advanced materials and nanocomposites due to its unique mechanical and structural properties. Understanding its mechanical behavior and the characteristics of silica nanoparticles is essential for optimizing their performance in various applications. This study numerically investigates the mechanical properties of amorphous silica material and the formation of silica nanoparticles using Molecular Dynamics (MD) simulations. Amorphous silica is generated from a crystalline structure through a melt-and-quench procedure. To determine its mechanical properties, six virtual mechanical tests are performed to compute the apparent elasticity tensor, from which the elastic moduli are extracted via an isotropic projection. The results indicate that amorphous silica exhibits nearly isotropic mechanical behavior, with high stiffness characterized by a bulk modulus of 36.84 GPa, a shear modulus of 30.49 GPa, a Young's modulus of 71.69 GPa, and a Poisson's ratio of 0.18. Additionally, the study explores the formation of silica nanoparticles with radii of 1.5 nm, 3.0 nm, and 4.8 nm. The analysis reveals that surface roughness increases as nanoparticle size decreases, which may have implications for interfacial interactions in composite materials. These findings contribute to the understanding of amorphous silica's mechanical behavior and its potential application as a reinforcing nanomaterial in polymer composites.

Keywords: mechanical properties, elasticity tensor, nanoparticles, molecular dynamics, amorphous silica, isotropic material

1. INTRODUCTION

Silica material has received a great deal of attention from researchers because of its importance in various applications such as composite reinforcement, electrical insulators, optical devices, and substrates in nano- and micro-electronic systems [1]. Due to good mechanical properties, magnetic strength, dielectric strength, thermal conductivity and selectivity for chemical modification, amorphous silica has become a key material in many fields [2] for instance structural composites, coatings, and nanomaterial applications. However, the amorphous structure has not been as thoroughly investigated as has crystalline silica [3].

From a mechanical point of view, amorphous silica nanoparticles are commonly used as nanofillers to reinforce polymer matrices [4]. The incorporation of silica nanoparticles can significantly enhance the mechanical strength, toughness, and thermal stability of polymer-based materials, making them widely applicable in structural composites, coatings, and biomedical materials. Despite the existence of several scales in nano-reinforced materials, small scales have not been fully explored, especially in terms of mechanical properties [5]. It is worth noting that interactions at small scales must be taken into account in multi-scale modeling of nano-reinforced materials, as they have not-insignificant effects on the macroscopic properties [6]. Various experimental studies have investigated local interactions at small scales (for instance between nanofillers and polymer chains in a polymer nanocomposite). For example, Berriot [7] and Papon [8] employed nuclear magnetic resonance to explore the matrix behavior near the surface of the nanofillers. Despite the widespread use, the mechanical response of silica nanofillers at the atomic and nanoscale levels remains a subject of ongoing research.

With the growth of computer simulation, various computational tools have been introduced to simulate materials at small scales. Among them, Molecular Dynamics (MD) simulation has been extremely widely used in recent years in materials science, as a powerful technique for understanding materials at atomic scale, especially for silica-based materials [9]. By simulating the deformation of amorphous silica under controlled loading conditions, MD allows for the determination of fundamental mechanical properties such as elastic moduli, bulk modulus, shear modulus, and Poisson's ratio. Previous studies have demonstrated the feasibility of MD in predicting the mechanical properties of amorphous materials. For instance, Vo et al. [10] investigated various factors that could affect the mechanical properties of amorphous silica such as boundary conditions, loading, size of domain, etc., using MD simulations. In another work, Yuan and Huang [11] have studied the tensile and brittle fracture behaviors of amorphous silica nanowire in an uniaxial tension. Later, Yuan and Huang [12] have performed MD simulations to investigate the influence of domain size on the elastic behavior of amorphous silica. However, further research is needed to assess the mechanical behavior of amorphous silica and validate its mechanical response through different virtual tests [1].

In addition to bulk material characterization, the formation and behavior of silica nanoparticles have gained significant attention, particularly in the context of nanocomposite materials [13]. Silica nanoparticles are commonly used as reinforcements in polymer matrices, where their surface properties and interaction with the surrounding matrix significantly affect the overall mechanical performance [13]. The structure and morphology of these nanoparticles, especially their surface roughness, play a crucial role in determining

interfacial adhesion and load transfer efficiency in composite materials [14]. Therefore, studying the formation of silica nanoparticles at the atomic scale is essential for optimizing their mechanical performance in engineering applications.

In this study, we use MD simulations to determine the mechanical properties of amorphous silica and prepare nanoparticles. The amorphous structure was obtained from α-quartz crystalline structure using a melt-and-quench process. The elasticity tensor of the material was obtained by means of a virtual testing procedure involving three tensile and three shear tests, respectively. Additionally, silica nanoparticles with varying sizes are generated to examine their structural characteristics and surface roughness. The results of this study contribute to a deeper understanding of the mechanical behavior of amorphous silica and its potential application as a reinforcing nanomaterial in polymer composites.

2. MATERIALS AND METHODS

2.1. Molecular dynamics simulation

Numerical techniques for atomistic simulation were developed at a very early stage by chemists and physicists. One of the first simulations was carried out by Allen et al. [15], which formed the basis for statistical mechanics simulations at atomic and molecular levels. The displacements of the particles in Metropolis's simulation were caused to evolve successively and randomly according to a criterion of conditioned probability [16]. The evolution of the particles over time alone is not a sufficient observation factor. Later, dynamic aspects were introduced into the particulate system by Allen et al. [15]; this paved the way for the development of Molecular Dynamics (MD). With MD, we can simulate the temporal evolution of the particle system by considering interactions between particles or between the system and the universe [17]. MD is now becoming one of the most widely used branches for understanding a broad range of phenomena in chemistry, physics and mechanics [18]. In this study, we focus on "classical" MD, where the potential field is determined empirically and the forces are derived from this potential field [19].

The main purpose of MD is to describe the dynamics of a group of particles based on Newton's laws as a function of time. Consider a system of N particles occupying a volume V in space. These particles have positions $\mathbf{r}^i$ and velocities $\mathbf{v}^i$, and consequently masses m^i (with i = 1, ..., N). Over time, the particles interact with one another within the system, and the system also interacts with its external environment. The method begins by initiating the system – mainly setting the initial positions and velocities of the particles, as well as the boundary conditions. Next, the total potential energy of the system is calculated from a given potential field on the interactions between the particles. Then, the forces and therefore the accelerations of each of the particles in the system are calculated. Newton's classic equations of motion are then integrated numerically in order to obtain the new positions and velocities of the particles, with pressure and temperature control in parallel. This procedure is looped until the system reaches equilibrium under certain conditions. Finally, the desired results are collected and analyzed. MD is a well-established method, further details of which are available in [20]. In this work, MD simulations were performed using LAMMPS code [21].

2.2. Method for generation of amorphous silica material

In this study, the amorphous structure of silica was created from crystalline silica using a melt-and-quench procedure (the crystalline structure was α-quartz, which is the most common polymorph of the silica minerals) [22]. The method is detailed below.

2.2.1. Atomistic description of crystalline silica structure

The α-quartz silica structure is made up of silicon (Si) and oxygen (O) atoms. Two interactions are taken into account for this atomic structure. The first is Van der Waals interaction, which is represented by a Buckingham potential [23]:

$$\Psi_{BCK}(r) = B_1 \exp\left(-\frac{r}{B_2}\right) - \frac{B_3}{r^6}, \quad (1)$$

where the parameters are as indicated in Table 1 below:

Table 1. Buckingham potential parameters for the simulation of atomic silica.

Interaction	**B_1**	**B_2**	**B_3**
Unit	eV	Å	eV/ Å^6
Si-Si	0	0.0657	0
Si-O	18003.7572	0.2052	133.5381
O-O	1388.7730	0.3622	175

The second interaction is Coulomb interaction, which is represented in the form [24]:

$$\Psi_{Coulomb}(r^{ij}) = \frac{q_i q_j}{4\pi\varepsilon_0 r^{ij}}, \quad (2)$$

where q_i and q_j are the electrical charges of the atom i and j respectively (q_{Si} = 2.4e and q_O = −1.2e, with e being the elementary charge of the proton), and ε_0 is the permittivity of the vacuum. The molar masses of Si and O are 28.0860 g/mol and 15.9994 g/mol respectively [25]. α-quartz silica is composed of unitary cells, each of which has geometric parameters including the cell lengths (denoted by (a, b, c)) and associated angles (denoted by (α, β, γ)) [26]. These parameters for the unitary cell are as follows: $a = b$ = 4.9137 Å, c = 5.4047 Å, $\alpha = \beta$ = 90°, and γ = 120°. The initial configuration of α-quartz is then created by assembling multiple cells to form a super cell, using the Pizza.py toolbox which is included in the LAMMPS code [21].

2.2.2. Procedure for generating amorphous silica structure

The α-quartz silica is first equilibrated at 300 K and 0 isotropic pressure, using the Nosé–Hoover thermostat to control temperature and pressure [27]. Then, the simulation box is heated to 10000 K, while keeping the pressure unchanged. This heating changes the structure from crystalline to molten. Finally, the temperature is returned to 100 K to obtain an amorphous structure. It should be noted that NPT treatment is applied to equilibrate the system (100 K temperature and 0 isotropic pressure). For more discussion on the transformation of crystalline silica to molten and finally to amorphous structure, readers can refer to [28].

2.2.3. Reduction of computational time: Method for obtaining equivalent elastic structure

The amorphous silica presented above, with the Buckingham and Coulomb potentials, is very costly in computation time, especially in terms of Coulomb potential [25]. In order to speed up the computation, therefore, we wish to replace all the interactions in atomic structure with their equivalent elastic interactions. Such elastic interactions were employed to maintain:

(i) the bond length between the Si and O atoms and (ii) the O–Si–O and Si–O–Si angles, respectively, as in the atomic structure. This approximation therefore allows us to preserve the amorphous structure of the silica, and also the mass density, the energy and – most importantly – the mechanical behavior. Furthermore, such replacement reduces the computation time.

To this end, tables describing the connection of the atoms were established, helping to assign the elastic bonds to be replaced. In the replaced amorphous structure, we used the elastic bonding potential:

$$\Psi_b(r) = \frac{1}{2} K_b \left(r - r_0 \right)^2, \tag{3}$$

and the elastic bending potential:

$$\Psi_\theta(\theta) = \frac{1}{2} K_\theta \left(\cos\theta - \cos\theta_0 \right)^2, \tag{4}$$

for the replacement (K_b, r_0, K_θ and θ_0 are the parameters, and r and θ are the variables of the models, respectively). In order to preserve the mass density, the geometry of the structure and the mechanical behavior, the parameters of the elastic potential models were identified on the basis of the initial amorphous structure.

2.3. Mechanical testing for obtaining elasticity tensor

As we are interested in the isotropic mechanical behavior of amorphous silica, boundary conditions were assigned to obtain the corresponding modulus of the material. For instance, a tensile test along the x_1 axis provided the Young's modulus E_1 of the material. Similarly, a shear test in the plane x_2x_3 measured the shear modulus μ_{23} of the material. However, as there is a non-negligible degree of noise in MD simulation, even for an isotropic material, the values of the moduli obtained do not entirely reflect the isotropic relationships. Consequently, in this study, the apparent elasticity tensor of the material was first measured by performing six virtual tests (three tensile and three shear tests, respectively) [29]. The apparent elasticity tensor is written as (in a matrix form):

$$\left[C^{app} \right] = \begin{bmatrix} C_{11} & C_{12} & C_{13} & C_{14} & C_{15} & C_{16} \\ & C_{22} & C_{23} & C_{24} & C_{25} & C_{26} \\ & & C_{33} & C_{34} & C_{35} & C_{36} \\ & & & C_{44} & C_{45} & C_{46} \\ & \text{Sym.} & & & C_{55} & C_{56} \\ & & & & & C_{66} \end{bmatrix} \tag{5}$$

Secondly, an isotropic projection was applied to the apparent elasticity tensor to obtain the isotropic elastic tensor, and therefore the elastic moduli of the material. The isotropic projection used to project the apparent tensor is detailed below, employed to obtain the bulk and shear modulus (denoted κ and μ, respectively) [30]:

$$\begin{cases} \kappa = \frac{11}{60}\left(C_{11} + C_{22}\right) + \frac{19}{30}C_{12} - \frac{1}{15}C_{33} \\ \mu = \frac{1}{5}\left(C_{11} + C_{22} + C_{33}\right) - \frac{2}{5}C_{12} \end{cases} \quad (6)$$

The isotropic elastic tensor could be then written as (note that the modified Voigt notation was used for the matrix representation of the elasticity tensor [31]):

$$\left[C^{iso}\right] = \begin{bmatrix} \kappa + 4\mu/3 & \kappa - 2\mu/3 & \kappa - 2\mu/3 & 0 & 0 & 0 \\ & \kappa + 4\mu/3 & \kappa - 2\mu/3 & 0 & 0 & 0 \\ & & \kappa + 4\mu/3 & 0 & 0 & 0 \\ & & & 2\mu & 0 & 0 \\ & \text{Sym.} & & & 2\mu & 0 \\ & & & & & 2\mu \end{bmatrix} \quad (7)$$

The relationships between the isotropic moduli could be written as

$$\kappa = \frac{E}{3(1-2\nu)}, \ \mu = \frac{E}{2(1+\nu)} \quad (8)$$

where E is the Young's modulus and ν is the Poisson's ratio of the material.

2.4. Formation of silica nanoparticles

In this study, silica nanoparticles were prepared from the elastic structure described above. In order to cut out the nanoparticles, a method based on realistic models containing silanol groups on the surface [32] was adopted. The nanoparticles comprised a spherical core (exhibiting similar structural characteristics to bulk silica), and a shell surrounding the core (containing silanol groups). For this purpose, five types of atoms were introduced, for the core (Si_n and O_n), and for the shell (Si_e, O_e^{c1} and O_e^{c2}), respectively. O_e^{c1} and O_e^{c2} represent oxygen atoms in the shell connected to one and two Si_e atoms, respectively. We use the notation R_p to represent the desired radius of the nanoparticle; R_{cp} represents the radius of the spherical core and therefore the thickness of the shell $e_e = R_p - R_{cp}$. It must be ensured that the thickness e_e of the shell has a minimum value of 0.9 nm [32].

- Load the elastic amorphous silica structure (index, positions, types (Si or O));
- Calculate radial distance between all atoms and the center of the simulation box (the center of the simulation box is the center of the nanoparticle);
- Remove all atoms outside of the sphere with a radius of R_p;
- Loop over all Si atoms to count, identify and store all neighboring O atoms (with a maximal radial distance of 0.19 nm);
- Remove all Si atoms having fewer than 4 neighboring oxygens previously identified, and located at a radial distance greater than R_{cp};
- Remove all O atoms in the shell (i.e. radius larger than R_{cp}), having no connection with Si atoms at a radial distance less than 0.19 nm;
- For the rest of oxygen atoms in the shell, identify O_e^{c1} atom type (having only one Si connection with a maximal distance of 0.19 nm), and O_e^{c2} atom type (having two Si connections with a maximal distance of 0.19 nm);
- Update the connectivity tables, indicating all atom types and connections.

Finally, the procedure allowed us to obtain amorphous silica nanoparticles with a given radius of R_p (a simulation box of amorphous silica larger than $2R_p$ should be used as input for the procedure from a geometric point of view).

2.5. Simulation setup and parameter summary

In this study, we attempted to generate three nanoparticles of R_p = 1.5, 3 and 4.8 nm, respectively. Such investigation could highlight the surface roughness of nanoparticles of different sizes. To this end, three α-quartz silica structures of 7×7×7, 14×14×14, and 30×30×30 unitary cells were generated, to obtain three nanoparticles of R_p = 1.5, 3 and 4.8 nm, respectively. Details of the configurations generated in the simulation are given in Table 2. Note that the length of the simulation box is larger than the diameter of the nanoparticles, as discussed previously. For the configurations of R_p = 1.5 and 3 nm, the simulation was repeated 20 times. However, for reasons of computation time, the largest silica box was simulated only once. Finally, it should be noted that the 30×30×30 cells configuration could be used to prepare nanoparticles of R_p = 1.5 and 3 nm. However, initial correlation could not be avoided.

Table 2. Summary of configurations generated.

Diameter of nanoparticle $2R_p$ (nm)	**3**	**6**	**9.6**
Unitary cells	7×7×7	14×14×14	30×30×30
Length of simulation box (nm)	**~3.6**	~6.9	~14.9
Number of runs	20	20	1

3. RESULTS AND DISCUSSION

3.1. Molecular Dynamics simulation of amorphous silica

3.1.1. Structural transition from crystalline to amorphous silica

As presented in Section 2.2.1, the α-quartz crystalline structure was generated for a configuration of 7×7×7 unitary cells. For simplicity's sake, an orthogonal simulation box was created in LAMMPS instead of a parallelepiped (i.e. the associated angle $\gamma = 120°$). The initial velocity distribution of the particles was generated based on a Gaussian distribution, the time step was set as 1 *fs* and the boundary condition was periodic. Details of the potential field are given in Table 1. As the transformation from crystalline to amorphous structure is detailed in Section 2.2.2, Figure 1 presents visualizations of that transformation. As can be seen, at the end of the procedure, an amorphous distribution of the atoms was obtained in the simulation box, while maintaining the structural characteristics (in terms of bond lengths and angles).

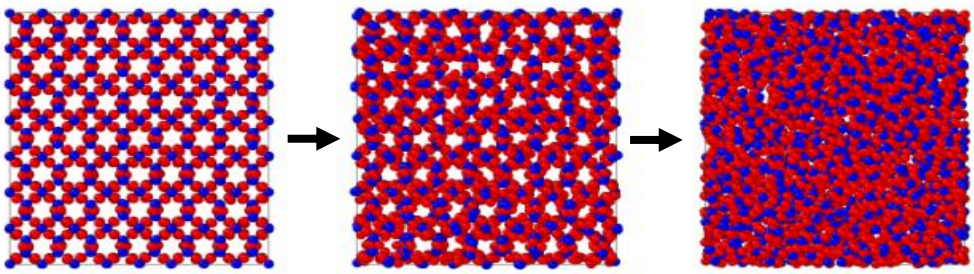

Figure 1. Visualization of transformation from crystalline to amorphous structure for a 7×7×7 unitary cell configuration.

3.1.2. Equivalent elastic model for amorphous structure

This section is devoted to the equivalent elastic model, introduced in Section 2.2.3, allowing us to replace the Buckingham and Coulomb potentials with elastic bonding and bending potentials. Based on the hypothesis of equivalence between crystalline and elastic structures equilibrated at 100 K and 0 isotropic pressure, the parameters introduced in Eqs. (3) and (4) were obtained as follows:

Table 3. Parameters of equivalent elastic models.

Potential	Bond	Parameter	Value	Unit
ψ_b	Si–O	K_b	57573.01	kcal/(mol.nm^2)
		r_0	0.1625	nm
ψ_θ	Si–O–Si	K_θ	95.6022	kcal/mol
		θ_0	145	°
	O–Si–O	K_θ	143.4034	kcal/mol
		θ_0	109.5	°

Using the values of the parameters indicated in Table 3, the equivalent elastic model exhibited an average Si–O bond length of 0.1625 nm, whereas that value for the initial amorphous structure was 0.161 nm. The average O–Si–O angle was about 110° and 112°, and the average Si–O–Si angle was about 150° and 140°, for the initial amorphous and equivalent structures, respectively. Note the strong correlation obtained to preserve the structural characteristics of the amorphous silica, while reducing computation cost (i.e. using elastic bonds instead of Coulomb interaction).

Finally, Table 4 summarizes the characteristics of all configurations in the simulation (also see Table 2) for amorphous silica using the equivalent elastic models. The mass density was 2452.42, 2441.93, and 2461.78 kg/m^3, for the configurations of 7×7×7, 14×14×14 and 30×30×30 unitary cells, respectively. These values were in accordance with the literature [32]. In terms of the geometric parameters of the simulation box, note that the lengths along the three axes are very similar. All configurations were ready for determination of mechanical properties and preparation of nanoparticles.

Table 4. Summary of simulations using equivalent elastic models.

Configuration	7×7×7 unitary cells	14×14×14 unitary cells	30×30×30 unitary cells
Number of runs	20	20	1
Lengths of simulation box	L_x=3.66 nm, L_y=3.59 nm, L_z=3.64 nm	L_x=6.85 nm, L_y=6.95 nm, L_z=7.06 nm	L_x=14.88 nm, L_y=14.90 nm, L_z=14.81 nm
Angles of simulation box	90°, 90°, 90°	90°, 90°, 90°	90°, 90°, 90°
Mass density	2452.42 kg/m^3	2441.93 kg/m^3	2461.78 kg/m^3

3.2. Mechanical properties: elasticity tensor and moduli

In this study, a loading rate of 0.5e^{-12} MPa/s was applied to test the mechanical properties of the amorphous silica (only for the 7×7×7 unitary cell configuration). It should be noted that this loading rate was chosen in relation both to computational time and to effect on the test

results. The test was conducted up to 0.1-0.15% of strain. Figure 2a presents the stress-strain relationships for three tensile tests along the x_1, x_2, and x_3 axes, while Figure 2b presents the stress-strain relationships for three shear tests on the x_1x_2, x_2x_3 and x_1x_3 planes. We clearly observe the isotropic mechanical behavior of amorphous silica, and its impressive stiffness.

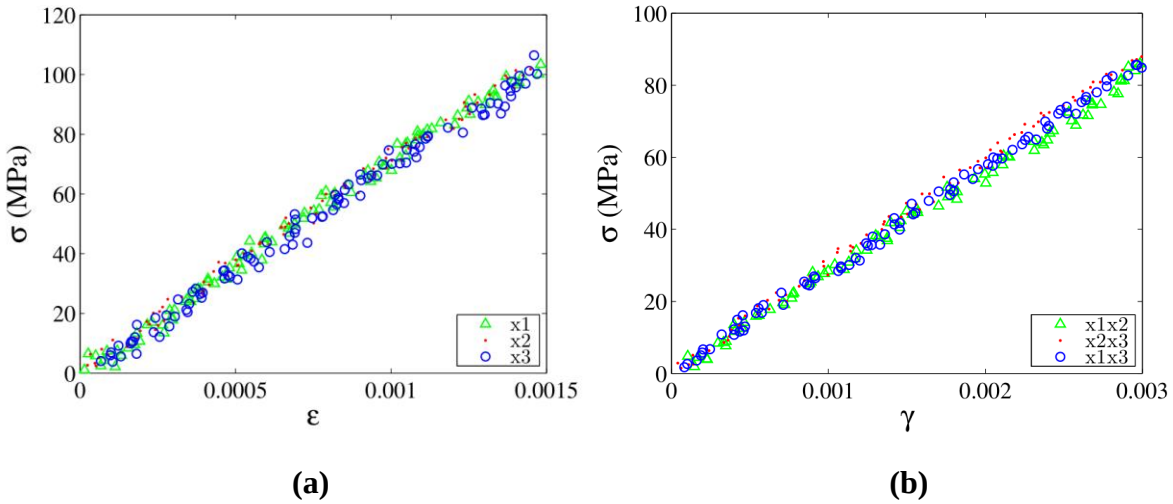

Figure 2. Stress-strain relationships for (a) three tensile tests along the x_1, x_2 and x_3 axes; (b) three shear tests on the planes x_1x_2, x_2x_3, and x_1x_3 at 100 K temperature.

By carrying out this sequence of virtual tests on the 20 configurations (listed in Table 2), the average value of the apparent elasticity tensor can be estimated as below (note that the modified Voigt notation was used for the matrix representation of the elasticity tensor [31]):

$$\left[C_{MD}^{app}\right] = \begin{bmatrix} 79.30 & 16.67 & 17.36 & 0.29 & 1.14 & 0.61 \\ & 77.17 & 14.80 & 1.53 & 0.66 & 1.07 \\ & & 77.48 & -1.08 & -0.23 & 1.14 \\ & & & 61.86 & 0.71 & -0.23 \\ & Sym. & & & 59.68 & 0.32 \\ & & & & & 59.95 \end{bmatrix} \quad (9)$$

The isotropic projection of the average apparent elastic tensor is given by

$$\left[C_{MD}^{iso}\right] = \begin{bmatrix} 77.48 & 16.51 & 16.51 & 0 & 0 & 0 \\ & 77.48 & 16.51 & 0 & 0 & 0 \\ & & 77.48 & 0 & 0 & 0 \\ & & & 60.97 & 0 & 0 \\ & Sym. & & & 60.97 & 0 \\ & & & & & 60.97 \end{bmatrix} \quad (10)$$

Table 5 compares the elastic constant for silica between this study and others reported in the literature. It should be noted that various parameters could affect the determination of mechanical properties, such as domain size, temperature, boundary and loading conditions [10]. Nonetheless, as observed in Table 5, our MD calculation yielded a good approximation of the behavior of amorphous silica using a substitution of the potentials.

Table 5. Comparison of mechanical properties with those determined in the literature.

Reference	Bulk modulus	Shear modulus	Young's modulus	Poisson's ratio
Notation	κ	μ	E	ν
Unit	GPa	GPa	GPa	-
Scholze [26]	37	31	73	0.17
Brown et al. [32]	28	26.3	54	0.223
Vo et al. [10]	98.99	26.53	73.052	0.377
Marcadon [33]	31.8	27	60	0.19
Freund and Suresh [34]	47.62	32.79	80	0.22
Deschamps et al. [35]	36.78	30.40	71.5	0.176
Hao and Hossain [36]	46.07-63.98	26.17-27.64	69.1	0.25-0.32
Chowdhury et al. [37]	112.12	26.62	74	0.39
Mei et al. [38]	49.02	23.15	60	0.296
This work	36.84	30.49	71.69	0.18

3.3. Structural and surface properties of silica nanoparticles

Using the procedure introduced in Section 2.4, five types of atoms constituting the silica nanoparticles were prepared; these are shown in Figure 3. Summary information for nanoparticles of radius of 1.5, 3 and 4.8 nm, respectively, is given in Table 6, showing the thickness of the shell, the radius of the spherical core, and the number of Si and O atoms.

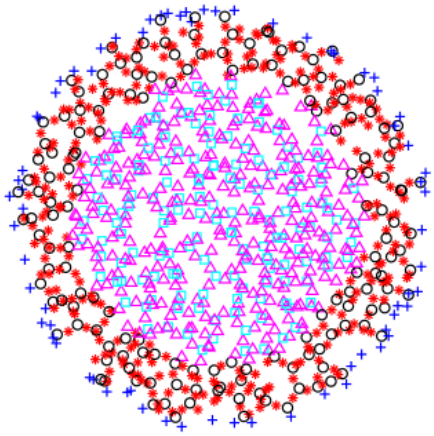

Figure 3. Silica nanoparticle (R_p=3 nm) with five types of atoms: purple triangle: O_n atom in the core; blue triangle: Si_n atom in the core; black circle: Si_e atom in the shell; red star: O_e^{c2} atom in the shell connected with two Si_e atoms; and blue plus sign: O_e^{c1} atom in the shell connected with one Si_e atom.

Table 6. Summary information of different nanoparticles.

Nanoparticle	Notation	R_p=1.5 nm	R_p=3 nm	R_p=4.8 nm
Shell thickness (nm)	e_e	0.9	0.9	0.9
Core radius (nm)	R_{cp}	0.6	2.1	3.9
Number of Si atoms		272	2460	10978
Number of O atoms		638	5331	23096
Total number of atoms		910	7791	34074

The three nanoparticles and their associated polyhedral mesh are shown in Figure 4. Note that the nanoparticles created have a certain roughness on their surface. It is seen in Figure 4 that the roughness increases when the size of the nanoparticle decreases from R_p=4.8 to R_p=1.5 nm. The same correlation was observed in various MD studies – for instance [39]. It should be noticed that such surface roughness can seriously affect the interaction between nanoparticles and the matrix in nanocomposites, such as polymer segments near the nanoparticles in nano-reinforced polymers [40]. Consequently, such surface roughness influences the macroscopic behavior of the nano-reinforced materials [41]. The preparation of nanoparticles in this study could be useful for mixing into a polymer matrix, with a view to investigating: (i) the local interaction of the matrix near the nanoparticles (interphase region, polymer chain conformation, mobility, mass density concentration, etc. [42]); and (ii) testing and modeling of the mechanical properties of the reinforced structures [43].

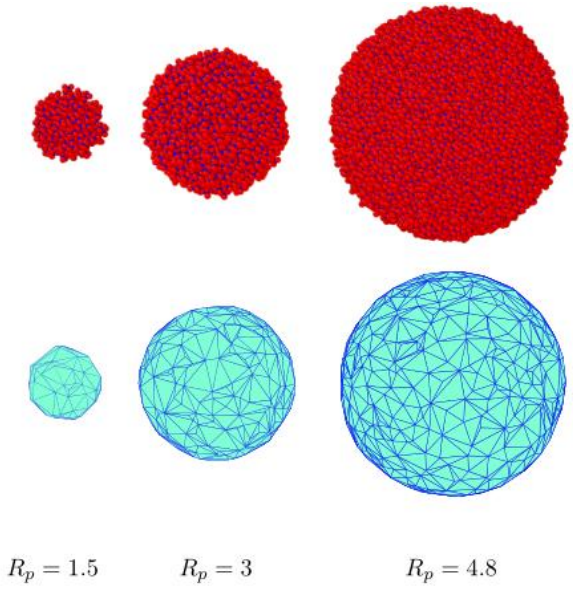

Figure 4. Visualization of three nanoparticles of different sizes and their associated polyhedral meshes. The silicon (Si) and oxygen (O) atoms appear in blue and red, respectively.

4. CONCLUSION

This study employed Molecular Dynamics (MD) simulations to characterize the mechanical properties of amorphous silica and to investigate the formation of silica nanoparticles. Amorphous silica was generated from an α-quartz crystalline structure using a melt-and-quench procedure, ensuring an atomistic configuration representative of experimental conditions. To optimize computational efficiency, an equivalent elastic potential model was developed to substitute the initial potential field while maintaining mechanical fidelity. The mechanical behavior of amorphous silica was examined through virtual mechanical testing, which revealed strongly isotropic properties with high stiffness. The material exhibited a bulk modulus of 36.84 GPa, shear modulus of 30.49 GPa, Young's modulus of 71.69 GPa, and Poisson's ratio of 0.18. Additionally, the formation of silica nanoparticles was investigated, leading to the successful preparation of three nanoparticle sizes (Rp = 1.5, 3, and 4.8 nm). The analysis indicated that surface roughness increased as

nanoparticle size decreased, which could significantly impact interfacial interactions in nanocomposites.

Future research could extend this work by investigating temperature and strain rate effects on the mechanical behavior of amorphous silica, providing a deeper understanding of its response under different loading conditions. Another promising direction involves molecular-scale simulations of silica-reinforced polymer nanocomposites, where the prepared nanoparticles can be embedded into various polymer matrices to analyze interfacial interactions and their influence on macroscopic material properties.

ACKNOWLEDGMENT

The authors would like to thank Prof. J. Guilleminot (Duke University, Durham, USA), for his helpful advice and comments on this paper. This research is funded by Vietnam National Foundation for Science and Technology Development (NAFOSTED) under grant number 107.02-2021.62.

REFERENCES

[1]. H. K. Issa, A. Taherizadeh, A. Maleki, A. Ghaei, Development of an aluminum/amorphous nano-SiO2 composite using powder metallurgy and hot extrusion processes, Ceramics International, 43 (2017) 14582–14592. https://doi.org/10.1016/j.ceramint.2017.06.057
[2]. K. Nadeem, F. Zeb, M. Azeem Abid, M. Mumtaz, M. Anis ur Rehman, Effect of amorphous silica matrix on structural, magnetic, and dielectric properties of cobalt ferrite/silica nanocomposites, Journal of Non-Crystalline Solids, 400 (2014) 45–50. https://doi.org/10.1016/j.jnoncrysol.2014.05.004
[3]. J. L. Gurav, I. K. Jung, H. H. Park, E. S. Kang, D. Y. Nadargi, Silica Aerogel: Synthesis and Applications, Journal of Nanomaterials, 2010 (2010) e409310. https://doi.org/10.1155/2010/409310
[4]. N. H. Khdary, M.E. Abdelsalam, Polymer-silica nanocomposite membranes for CO2 capturing, Arabian Journal of Chemistry, 13 (2020) 557–567. https://doi.org/10.1016/j.arabjc.2017.06.001
[5]. H. K. Issa, A. Taherizadeh, A. Maleki, Atomistic-level study of the mechanical behavior of amorphous and crystalline silica nanoparticles, Ceramics International, (2020). https://doi.org/10.1016/j.ceramint.2020.05.272
[6]. H. L. Quang, Q. C. He, Variational principles and bounds for elastic inhomogeneous materials with coherent imperfect interfaces, Mechanics of Materials, 40 (2008) 865–884. https://doi.org/10.1016/j.mechmat.2008.04.003
[7]. J. Berriot, F. Lequeux, L. Monnerie, H. Montes, D. Long, P. Sotta, Filler–elastomer interaction in model filled rubbers, a 1H NMR study, Journal of Non-Crystalline Solids, 307–310 (2002) 719–724. https://doi.org/10.1016/S0022-3093(02)01552-1
[8]. A. Papon, K. Saalwächter, K. Schäler, L. Guy, F. Lequeux, H. Montes, Low-Field NMR Investigations of Nanocomposites: Polymer Dynamics and Network Effects, Macromolecules, 44 (2011) 913–922. https://doi.org/10.1021/ma102486x
[9]. Y. Jing, Q. Meng, Molecular dynamics simulations of the mechanical properties of crystalline/amorphous silicon core/shell nanowires, Physica B: Condensed Matter, 405 (2010) 2413–2417. https://doi.org/10.1016/j.physb.2010.02.056
[10]. T. Vo, B. Reeder, A. Damone, P. Newell, Effect of Domain Size, Boundary, and Loading Conditions on Mechanical Properties of Amorphous Silica: A Reactive Molecular Dynamics Study, Nanomaterials, 10 (2020) 54. https://doi.org/10.3390/nano10010054
[11]. F. Yuan, L. Huang, Molecular dynamics simulation of amorphous silica under uniaxial tension: From bulk to nanowire, Journal of Non-Crystalline Solids, 358 (2012) 3481–3487. https://doi.org/10.1016/j.jnoncrysol.2012.05.045

[12]. F. Yuan, L. Huang, Size-dependent elasticity of amorphous silica nanowire: A molecular dynamics study, Appl. Phys. Lett., 103 (2013) 201905. https://doi.org/10.1063/1.4830038
[13]. H. K. Issa, A. Taherizadeh, A. Maleki, Atomistic-level study of the mechanical behavior of amorphous and crystalline silica nanoparticles, Ceramics International, 46 (2020) 21647–21656. https://doi.org/10.1016/j.ceramint.2020.05.272
[14]. O. Oguz, N. Candau, S. H. F. Bernhard, C. K. Soz, O. Heinz, G. Stochlet, C. J. G. Plummer, E. Yilgor, I. Yilgor, Y.Z. Menceloglu, Effect of surface modification of colloidal silica nanoparticles on the rigid amorphous fraction and mechanical properties of amorphous polyurethane–urea–silica nanocomposites, Journal of Polymer Science Part A: Polymer Chemistry, 57 (2019) 2543–2556. https://doi.org/10.1002/pola.29529
[15]. M. P. Allen, D. J. Tildesley, Computer Simulation of Liquids, Clarendon Press, 1989.
[16]. K. Binder, Monte Carlo and Molecular Dynamics Simulations Polymer, Oxford University Press, Inc., USA, 1995.
[17]. W. K. Liu, E. G. Karpov, H. S. Park, Nano Mechanics and Materials: Theory, Multiscale Methods and Applications, 1 edition, Wiley, Chichester, England; Hoboken, NJ, 2006.
[18]. D. C. Rapaport, The Art of Molecular Dynamics Simulation, 2 edition, Cambridge University Press, Cambridge, UK 2004.
[19]. A. Satoh, Introduction to Practice of Molecular Simulation: Molecular Dynamics, Monte Carlo, Brownian Dynamics, Lattice Boltzmann and Dissipative Particle Dynamics, 1 edition, Elsevier, Amsterdam 2010.
[20]. D. Frenkel, B. Smit, Understanding Molecular Simulation: From Algorithms to Applications, 2 edition, Academic Press, San Diego, 2001.
[21]. S. Plimpton, Fast Parallel Algorithms for Short-Range Molecular Dynamics, Journal of Computational Physics, 117 (1995) 1–19. https://doi.org/10.1006/jcph.1995.1039
[22]. S. Tsuneyuki, Molecular dynamics simulation of silica with a first-principles interatomic potential, Mol Eng, 6 (1996) 157–182. https://doi.org/10.1007/BF00161726
[23]. B. W. H. van Beest, G. J. Kramer, R. A. van Santen, Force fields for silicas and aluminophosphates based on ab initio calculations, Phys. Rev. Lett., 64 (1990) 1955–1958. https://doi.org/10.1103/PhysRevLett.64.1955
[24]. A. Carré, L. Berthier, J. Horbach, S. Ispas, W. Kob, Amorphous silica modeled with truncated and screened Coulomb interactions: A molecular dynamics simulation study, J. Chem. Phys., 127 (2007) 114512. https://doi.org/10.1063/1.2777136
[25]. W. Gonçalves, J. Morthomas, P. Chantrenne, M. Perez, G. Foray, C.L. Martin, Molecular dynamics simulations of amorphous silica surface properties with truncated Coulomb interactions, Journal of Non-Crystalline Solids, 447 (2016) 1–8. https://doi.org/10.1016/j.jnoncrysol.2016.05.024
[26]. H. Scholze, Glass: nature, structure, and properties, Springer-Verlag, 1991
[27]. S. Nosé, A unified formulation of the constant temperature molecular dynamics methods, J. Chem. Phys., 81 (1984) 511–519. https://doi.org/10.1063/1.447334
[28]. K. Vollmayr, W. Kob, K. Binder, Cooling-rate effects in amorphous silica: A computer-simulation study, Phys. Rev. B, 54 (1996) 15808–15827. https://doi.org/10.1103/PhysRevB.54.15808
[29]. C. Soize, Tensor-valued random fields for meso-scale stochastic model of anisotropic elastic microstructure and probabilistic analysis of representative volume element size, Probabilistic Engineering Mechanics, 23 (2008) 307–323. https://doi.org/10.1016/j.probengmech.2007.12.019
[30]. J. Guilleminot, C. Soize, Generalized stochastic approach for constitutive equation in linear elasticity: a random matrix model, International Journal for Numerical Methods in Engineering, 90 (2012) 613–635. https://doi.org/10.1002/nme.3338
[31]. S. C. Cowin, M. M. Mehrabadi, The structure of the linear anisotropic elastic symmetries, Journal of the Mechanics and Physics of Solids, 40 (1992) 1459–1471. https://doi.org/10.1016/0022-5096(92)90029-2
[32]. D. Brown, V. Marcadon, P. Mélé, N. D. Albérola, Effect of Filler Particle Size on the Properties of Model Nanocomposites, Macromolecules, 41 (2008) 1499–1511. https://doi.org/10.1021/ma701940j

[33]. V. Marcadon, Effets de taille et d'interphase sur le comportement mécanique de nanocomposites particulaires., phdthesis, Ecole Polytechnique X, 2005. https://pastel.archives-ouvertes.fr/pastel-00001804 (accessed June 5, 2020).
[34]. L. B. Freund, S. Suresh, Thin Film Materials: Stress, Defect Formation and Surface Evolution, Cambridge University Press, 2004.
[35]. T. Deschamps, J. Margueritat, C. Martinet, A. Mermet, B. Champagnon, Elastic Moduli of Permanently Densified Silica Glasses, Scientific Reports, 4 (2014) 7193. https://doi.org/10.1038/srep07193
[36]. T. Hao, Z. M. Hossain, Atomistic mechanisms of crack nucleation and propagation in amorphous silica, Phys. Rev. B, 100 (2019) 014204. https://doi.org/10.1103/PhysRevB.100.014204
[37]. S. C. Chowdhury, E. A. Wise, R. Ganesh, J. W. Gillespie, Effects of surface crack on the mechanical properties of Silica: A molecular dynamics simulation study, Engineering Fracture Mechanics, 207 (2019) 99–108. https://doi.org/10.1016/j.engfracmech.2018.12.025
[38]. H. Mei, Y. Yang, A. C. T. van Duin, S. B. Sinnott, J. C. Mauro, L. Liu, Z. Fu, Effects of water on the mechanical properties of silica glass using molecular dynamics, Acta Materialia, 178 (2019) 36–44. https://doi.org/10.1016/j.actamat.2019.07.049
[39]. Y. Takato, M. E. Benson, S. Sen, Small nanoparticles, surface geometry and contact forces, Proceedings of the Royal Society A: Mathematical, Physical and Engineering Sciences, 474 (2018) 20170723. https://doi.org/10.1098/rspa.2017.0723
[40]. D. Surblys, Y. Kawagoe, M. Shibahara, T. Ohara, Molecular dynamics investigation of surface roughness scale effect on interfacial thermal conductance at solid-liquid interfaces, J. Chem. Phys., 150 (2019) 114705. https://doi.org/10.1063/1.5081103
[41]. V. Marcadon, D. Brown, E. Hervé, P. Mélé, N. D. Albérola, A. Zaoui, Confrontation between Molecular Dynamics and micromechanical approaches to investigate particle size effects on the mechanical behaviour of polymer nanocomposites, Computational Materials Science, 79 (2013) 495–505. https://doi.org/10.1016/j.commatsci.2013.07.002
[42]. S. Yu, S. Yang, M. Cho, Multi-scale modeling of cross-linked epoxy nanocomposites, Polymer, 50 (2009) 945–952. https://doi.org/10.1016/j.polymer.2008.11.054
[43]. J. Choi, H. Shin, S. Yang, M. Cho, The influence of nanoparticle size on the mechanical properties of polymer nanocomposites and the associated interphase region: A multiscale approach, Composite Structures, 119 (2015) 365–376. https://doi.org/10.1016/j.compstruct.2014.09.014